The influence of finite depth on the evolution of extreme wave statistics in numerical wave tanks

Tianning Tang[a,1], Thomas A. A. Adcock[a]

[a]*Department of Engineering Science, University of Oxford, Oxford, UK*

Abstract

Model tests with unidirectional random wave fields are common for coastal engineering purposes. In this paper, we investigate the finite water depth effect on both the probability of extreme events and the averaged shape of them in such experimental conditions. We simulate some typical model test conditions with a numerical tool, which solves the fully non-linear wave equations. We find the analytical solution based on Nonlinear Schrödinger equation (NLS) to be accurate for low steepness and relatively deep water cases. However, the analytical solution underestimates the kurtosis at the steady state for high steepness cases in shallow water, and also gives zero value of kurtosis at critical water depth, whereas a small but non-zero value of kurtosis is observed in the numerical tank. We also investigate the averaged shape of the extreme events, which are modified by nonlinear physics over the distance. The horizontal asymmetry is significant initially but is greatly reduced to a steady state, and the contraction of the wave groups grows monotonically until the steady state is reached along the wave tank. Finite water depth has limited effects on the averaged shape of large events, especially for the extremely steep waves.

Keywords: Surface wave, Rogue wave

[1]Email: tianning.tang@some.ox.ac.uk

1. Introduction

Coastal engineers often need to perform model tests in unidirectional wave flumes. To simulate the short-term wave variability in nature they will do tests using random waves with a predefined spectrum. Typically, waves will be generated by randomly assigning a phase to different Fourier components, and using this as a basic model to drive the paddle (possibly including second order physics see [1]). However, in unidirectional waves, non-linear interactions lead to correlations forming between components, increasing the number of large waves and modifying the shape of the average event away from that predicted in a linear model. This contrasts to waves in the real ocean which are directionally spread. In such realistic seas, where the wave field is in 'equilibrium', models based on linear dynamics are expected to be good predictors of wave height [2, 3] and of group shape for all but the most extreme waves [4, 5].

It is important for testing models that this departure from linear statistics is understood. For instance, if the tester simulates a design sea state at the paddle, the loads predicted on the object being tested will be over-estimated if the non-linear physics has led to more large waves. Further, the shape of the extreme wave-group can be important in determining forces. A clear example of this is in structures which have a dynamics response such as the 'ringing' effect which may impact the design of offshore wind turbines [6, 7]. Thus, model testers need to be able to assess the importance of these change in the shape of extremes in their work.

The theoretical work on this problem perhaps originates with the pioneering work of Benjamin and Feir [8]. However, analysis of the problem looking at the evolution of wave from an initially random initial condition stems from the work of Janssen [9] with major theoretical contributions from [10, 3, 11, 12, 13]. Experiments and numerics such as [14, 15, 16, 17] examine the multidimensional random wave fields and mainly focus on deep water waves. Most of this work has focussed on the amplitude distribution of waves rather than the shape of extreme wave groups.

In finite water depth, the wave-induced current stabilise the nonlinear focusing for unidirectional wave trains at sufficiently small relative water depths below a critical value of $k_0 d = 1.363$ [18, 19, 20] and the cubic nonlinearity vanishes [21] in nonlinear Schrödinger equation (NLS) type solutions. However, nonlinear focusing can still be triggered with directional disturbances in finite water depth (see numerical simulations in [22, 23] and experiments in [24]). The role of directionality in finite water depth in wave statistics of random wave fields have been examined by [25] with experimental results and numerical simulations (see also [26] and experiments in [27]).

Kurtosis of the free surface is widely used as a proxy for the distribution of extreme waves (see for instance [10]). Unfortunately, most of the closed-form analytical predictions on the evolution of kurtosis focus on deep water waves, which excludes the suppression of nonlinear wave focussing in finite water depth. In the present paper, we apply a simple depth correction to the existing analytical model and investigate its validity when including finite depth effects. We numerically explore what happens to steep sea-states as they evolve from uncorrelated initial conditions to an equilibrium state and how the shape of the largest waves varies along the flume using a fully non-linear potential flow solver.

2. Numerical experiments

2.1. The model

To investigate the wave evolution in different water depths, OceanWave3D is used to solve the standard fully non-linear wave equations (see [28] for details). This numerical scheme solves the potential flow governing equations over the whole domain with fully non-linear boundary conditions at the free surface using a finite difference method.

The numerical wave tank has a length of 320 m in the wave propagation direction with 4098 nodes, which provides a spatial resolution of 0.078 m (approximately 23 nodes per peak wavelength). Fifteen clustered nodes are used

vertically in the water column. We have been careful to mitigate the impact of different grid resolutions on our results and have ensured the numerical accuracy of the results following the approach of [29]. The total simulation time is 1920 s with a time step of 0.02 s (75 per period).

Waves are generated with a relaxation zone in the first 30 m of the numerical wave tank and are absorbed by a 35 m long pressure damping zone at the end. Care has been taken to ensure the second order error waves and wave reflection effects are negligible. There is a local smoothing filter to model the wave breaking effects. This local filter activates when the vertical Lagrangian acceleration on the free surface is greater than 0.4 m/s^2. When this filter is triggered, a small amount of energy is removed from the breaking waves locally until the vertical particle acceleration is below the threshold. For the case of deep water, the model agrees very well the experimental results [30].

2.2. Test conditions

The input wave spectrum for the tests conditions, is a TMA transform as proposed by Hughes [31]:

$$S(f)_D = \frac{S(f)_\infty}{2n} \tanh^2 k_0 d, \tag{1}$$

where $S(f)_D$ is the transformed finite water depth spectrum, $S(f)_\infty$ is the spectrum for a deep water conditions, n is the ratio between group velocity and phase velocity at water depth of d and k_0 is the dominant wave number. This transform retains the spectral shape in deep water but accounts for the notional influence of linear shoaling on all the components. For $S(f)_\infty$, we used a JONSWAP spectrum with $\gamma = 3.3$. A recent study shows this TMA transformed JONSWAP spectrum predicts the averaged shape of extreme events well in intermediate water depth [32]. We consider two cases in this paper. The main difference between them is the significant wave height. Case 1 has a higher significant wave height of 0.14 m (steepness (ϵ) $= 2\pi H_s/(gT_0^2) = 0.04$), and case 2 have a significant wave height of 0.11 m (steepness (ϵ) $= 0.03$). We summarise the sea state parameters in Table 1:

Table 1: Sea state parameters for both cases.

No.	T_0 [s]	k_0 [m^{-1}]	d [m]	$k_0 d$	H_s [m]	ϵ
Case 1 No. 1	1.5	2.06	0.65	1.33	0.14	0.04
Case 1 No. 2	1.5	1.97	0.77	1.5	0.14	0.04
Case 1 No. 3	1.5	1.82	1.33	2.42	0.14	0.04
Case 1 No. 4	1.5	1.80	1.75	3.14	0.14	0.04
Case 2 No. 1	1.5	2.06	0.65	1.33	0.11	0.03
Case 2 No. 2	1.5	1.97	0.77	1.5	0.11	0.03
Case 2 No. 3	1.5	1.82	1.33	2.42	0.11	0.03
Case 2 No. 4	1.5	1.80	1.75	3.14	0.11	0.03

3. Results

In this section, we aim at investigating the evolution of the probability of the extreme events and the averaged shape of these. We first compare the numerical results with analytical results for the evolution of dynamic excess kurtosis based on the NLS [12] in different water depths. We further investigate the average shape of largest events by quantifying the horizontal asymmetry and the contraction of the wave envelope in the mean wave direction at different water depths.

3.1. Evolution of dynamic kurtosis

We start by comparing our numerical results with modified theoretical predictions based on [12]. We compute the dynamic kurtosis C_4^d, which is suggested by Janssen [9] as a parameter for estimating rogue wave density:

$$C_4^d = \frac{\langle \eta_L^4 \rangle}{3\mathrm{std}^4} - 1, \tag{2}$$

where η_L is the linearised free surface elevation with respect to the mean water level, std is the standard deviation of the free surface, and angle brackets denote a statistical average. We 'correct' the simulated free surface for bound waves

by removing all the harmonics that do not follow the dispersion relationship in the frequency domain (see [33] for details).

Mori and Janssen [10] present the evolution of excess kurtosis for unidirectional waves in deep water with a three-dimensional integral evolution equation (their Eq. (14)) and a simplified version in the narrow-bandwidth and large-time limit for Gaussian spectra (their Eq. (28)). Without invoking the large-time assumptions, the integral can be evaluated in closed-form [12] (see also [13])

$$\frac{C_4^d(x)}{\mathrm{BFI}^2} = \frac{\pi}{3\sqrt{3}}\Big[1 - \frac{6}{\pi}\mathrm{Im}\Big(i \arcsin\frac{1+2i\alpha}{2}\Big)\Big], \tag{3}$$

where C_4^d is the dynamic excess kurtosis, Im is the imaginary part, $\alpha = 2\nu^2 x/\lambda_0$ and ν is the bandwidth of the wave spectrum.

However, Equation 3 is derived for deep water waves. To obtain the finite water corrections, we simplistically follow Serio's method of computing Benjamin-Feir Index (BFI) in finite water depth [34]:

$$BFI = \sqrt{m_0} k_p Q_p \kappa \sqrt{2\pi}, \tag{4}$$

where $m_0 = H_s^2/16$ is the zeroth moment of the energy spectrum, κ is a depth correction factor, which is unity in deep water. κ can be computed as:

$$\kappa = \mu\sqrt{\frac{|\tau|}{\chi}}, \tag{5}$$

where μ, τ and χ are all dimensionless coefficients depending on relative water depth $k_p d$. The general forms of μ, τ and χ are (see [35] for detailed derivation):

$$\mu = 1 + 2\frac{k_p d}{\sinh(2k_p d)}, \tag{6}$$

$$\tau = -\mu^2 + 2 + 8(k_p d)^2 \frac{\cosh(2k_p d)}{\sinh^2(2k_p d)}, \tag{7}$$

$$\chi = \frac{\cosh(4k_p d) + 8 - 2\tanh^2(k_p d)}{8\sinh^4(k_p d)} - \frac{(2\cosh^2(k_p d) + 0.5\mu)^2}{\sinh^2(2k_p d)\Big[\frac{k_p d}{\tanh(k_p d)} - \Big(\frac{\mu}{2}\Big)^2\Big]}. \tag{8}$$

Q_p is the quality factor introduced by [36]. Q_p is a dimensionless parameter, which describes the spectral bandwidth. It has less sensitivity to the high frequency tail of the spectrum (and cut-off frequency) than other bandwidth metrics [34, 37]. Q_p is given by:

$$Q_p = \frac{2}{{m_0}^2} \int_0^\infty f S^2(f) \mathrm{d}f, \tag{9}$$

where $S(f)$ is the wave spectral density function.

Figure 1 shows the evolution of dynamic excess kurtosis (C_4^d) at different water depths. From Figure 1, both numerical simulations and the analytical solution based on cubic nonlinear Schrödinger equation (NLS) start with excess kurtosis of zero. The excess kurtosis reduced noticeably as the water depth decreases towards the critical value, which agrees well with the existing literature on the suppression of nonlinear focussing at finite water depth [18, 19, 20]. The asymptotic analysis captured the overall trends except for the shallowest case ($k_0 d = 1.33$). Near the critical water depth of $k_0 d = 1.36$ where the cubic nonlinearity vanishes [21] meaning the analytical solution predicts that the free surface remains Gaussian (excess kurtosis is always zero). However, we still observe a small value of dynamic excess kurtosis at steady state, which is consist ant with previous experiments and numerics [25]. This could be due to the imperfections in correcting for bound waves, but is also likely to be due to nonlinearity beyond the cubic nonlinearity contributing to the excess kurtosis. This could also explain the small gap between the theoretical predictions and the simulated results for the case with $k_0 d = 1.5$. For relative deep water cases ($k_0 d = 2.41$ and $k_0 d = 3.14$), the numerical results agree well with the analytical solutions, which suggests the asymptotic analysis can provide an accurate estimation of kurtosis for low steepness and relatively deep water wave fields.

We further investigate the evolution of kurtosis at the same water depths but with higher wave steepness in Figure 2. For the relatively deep water case ($k_0 d = 3.14$), the analytical solution predicts the initial growth of the excess kurtosis well, but after the peak, numerical results depart from the theoretical solutions with a decreasing trend. This could be due to the inherent limitations of the

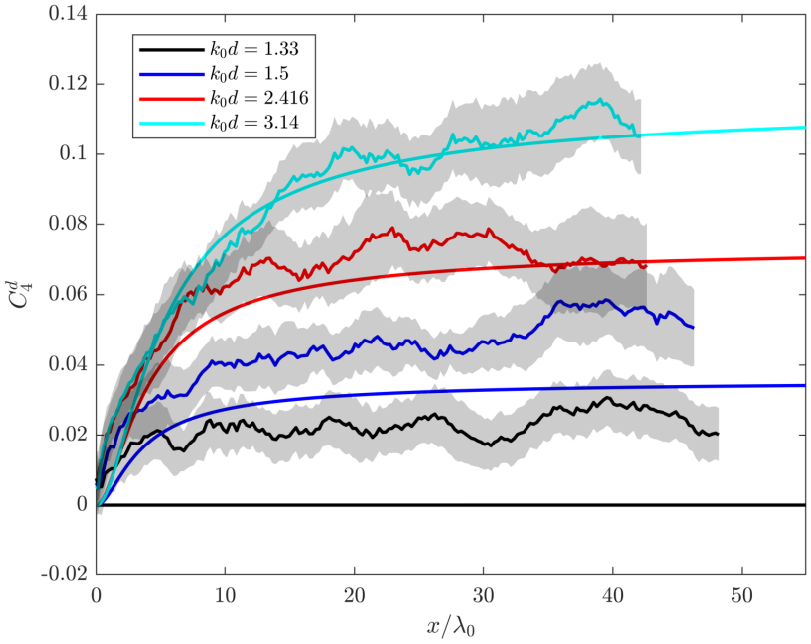

Figure 1: Evolution of dynamic excess kurtosis for case 2 along the numerical flume with different water depth. The dashed line shows the corresponding theoretical predictions from [12] for each water depth.

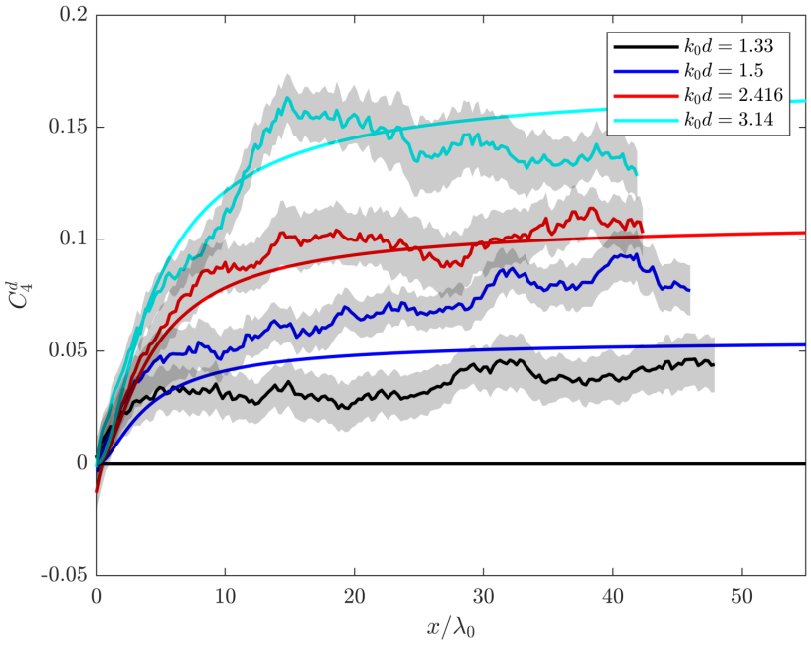

Figure 2: Evolution of dynamic excess kurtosis for case 1 along the numerical flume with different water depth. The dashed line shows the corresponding theoretical predictions from [12] for each water depth.

NLS typed approximations, which assume a narrowbanded Gaussian spectrum. However, at the initial stage of wave propagation, the spectrum broadens as the correlations between initially uncorrelated components develop (see [38] for example). This introduces permanent changes to the wave spectrum. The assumption that kurtosis can be expressed in terms of lower-order moments (Eq. (16) of [9]) may also become invalid if the waves are too steep. The discrepancies in excess kurtosis, for relatively shallow water case ($k_0d = 1.36$) increase for higher steepness. This is expected as the contribution from higher order nonlinearity should become more significant for high steepness cases.

3.2. Contribution of bound waves

In the above we focus on the free waves as a surrogate measure of the correlation between freely propagating components in our numerical simulations. We quantify the contribution from nonlinear interactions between free waves by examining the spatial evolution of dynamic excess kurtosis (C_4^d). However, for real water waves, the contribution to kurtosis induced by the bound waves can be significant, especially at finite water depth [39, 40, 10]. The bound wave contribution to kurtosis, C_4^b, can be approximated by subtracting dynamic excess kurtosis from the excess kurtosis of original surface elevation:

$$C_4^b = \frac{\langle \eta^4 \rangle}{3\mathrm{std}^4} - 1 - C_4^d, \tag{10}$$

Janssen [41] and Fedele [3] shows that for deep water waves, the bound wave contribution to kurtosis, as an independent value of space, can be approximated as:

$$C_4^b = C_4^b|_{ss} = 6(k_0\ std)^2. \tag{11}$$

In this section, we examine the steady-state value of bound wave contribution to kurtosis ($C_4^b|_{ss}$), which is approximated as the average value of last ten wave lengths in the numerical tank. From Figure 3, in relatively shallow water, the bound wave contribution to kurtosis increases significantly. This agrees well with the previous studies [39]. On the deep water side, the theoretical predictions agrees extremely well with the simulated results for Case 2. The discrepancy between these for Case 1 could be due to the dynamic kurtosis departing from the theoretical predictions (see Figure 2). Unsurprisingly, Wave steepness also has a significant impact on the bound wave contribution as the contribution ratio for Case 1 is generally higher than Case 2.

3.3. Averaged shape of the extreme waves

The linear wave theory suggests the average shape of the largest event is given by the scaled autocorrelation function [42, 43, 44]. This approach has

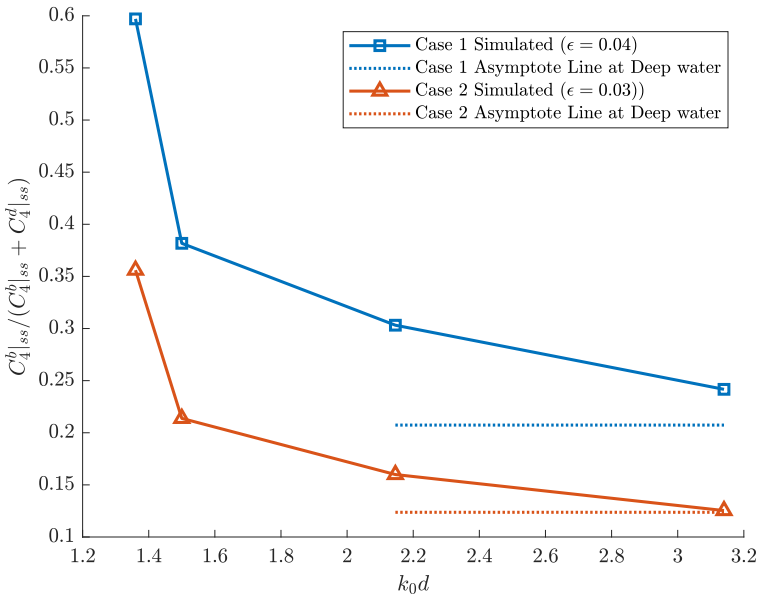

Figure 3: Contribution ratio from bound waves to kurtosis at steady state for different relative water depths for both Case 1 and Case 2. Solid lines shows the simulation results and dashed lines indicates the theoretical value obtained from Equation 11.

been referred to as NewWave (primarily in the engineering community) and as the theory of quasi-determinism (primarily in the physics community). The expected shape of an extreme event with the amplitude of the peak (at $t = 0$) scaled to unity is given by:

$$\eta(t) = \frac{1}{m_0} \int_0^\infty S(f) \cos(2\pi f t) \mathrm{d}f, \tag{12}$$

where $S(f)$ is the wave spectrum, $m_0 = H_s^2/16$ is the zeroth moment of the wave spectrum. However, the nonlinear physics might modify the shape of these extreme events. For deep-water waves, nonlinear changes on the shape of extreme events have been investigated for wave groups and random seas (see [45]). Adcock and Taylor [46] shows that the group would contract spatially according to the analytical results based on NLS. For unidirectional random waves, the work of [47] and [48] looked at the averaged shapes of extreme events in deep water and the recent work of [49] investigates these extreme events in finite water depth.

We herein present the change in the averaged shape of the extreme events (in the time-domain) and look at how this changes as the waves evolve spatially along the wave tank. Figure 4 shows the averaged free surface of the largest events at different positions in the numerical tank. When the waves are being generated, the wave group is symmetric horizontally as predicted by the linear theory. Nonlinear physics modifies the shape of these largest events as the wave propagates along the wave tank. From Figure 4, two main modifications from nonlinear physics are that the largest wave tends to move to the front of the wave group (horizontal asymmetry) and the contraction of the wave group. The finite water depth seems to have limited impact on the averaged shape of extreme events. The results presented here have had the bound harmonics removed to facilitate easier comparison with linear theory and between water depths.

We quantify the change of the extreme events with two parameters (see [4] for details). The first parameter measures the width of the wave group and the second parameter measures the wave group asymmetry. From Figure 5,

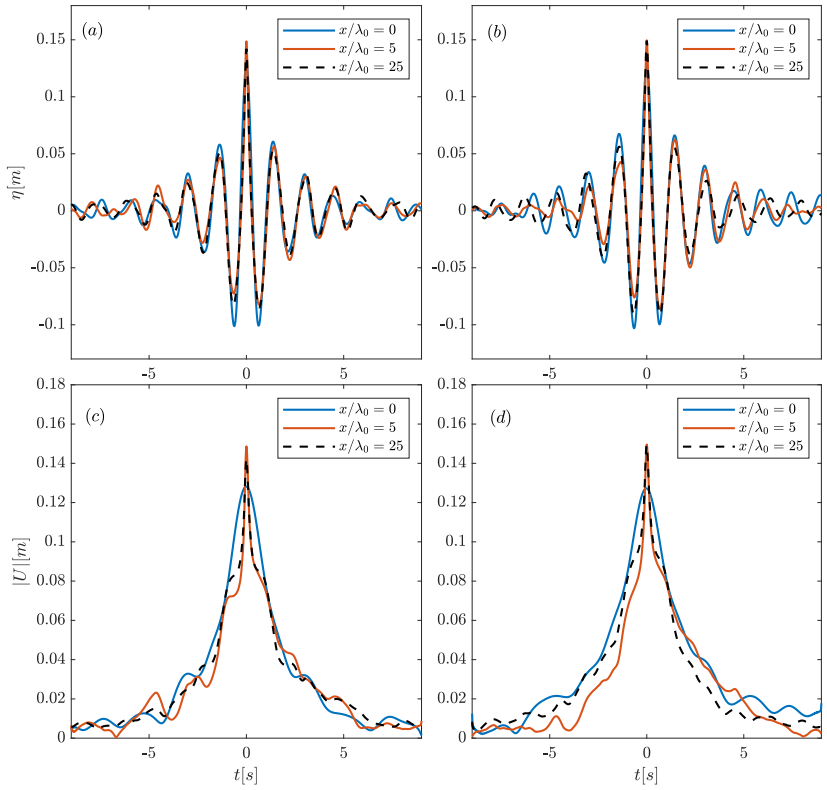

Figure 4: Average shape of the 5 largest crest profiles (a, b) and the corresponding envelope profiles (c, d) out of over 1280 waves at $x/\lambda_0 = 0, 5, 25$ for random waves with a, c: $k_0 d = 1.33$ and b, c: $k_0 d = 3.14$.

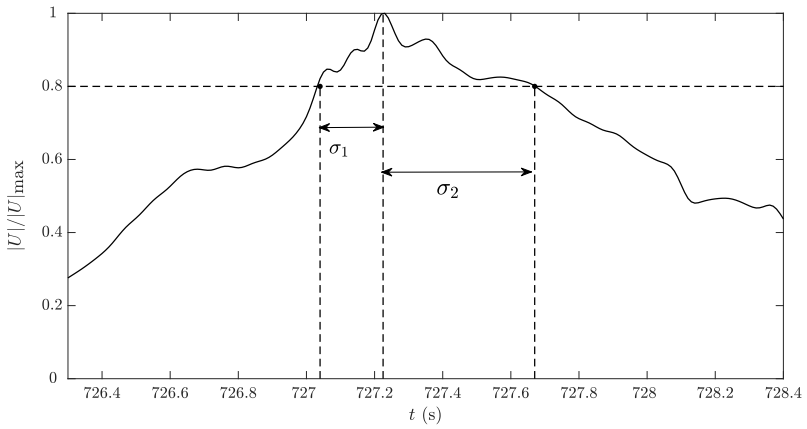

Figure 5: Illustration of the envelope duration when the normalised envelope height $|U|\,/\,|U|_{\max}$ exceeds 80% of its peak height.

σ_1 and σ_2 is defined as the duration when the envelope height exceeds 80% of the maximum height of the envelope averaged from top 20 or 5 largest extreme events from a 32 minutes simulations. The wave envelope is calculated using a Hilbert transform:

$$|U| = \sqrt{\eta^2 + \eta_H^2}, \tag{13}$$

where $|U|$ is the wave envelope and η_H is the Hilbert transformed surface elevation.

We define the parameters B_1 and B_2 to be the ratios between the measured averaged duration σ_1 and σ_2 and the duration that would be predicted by the linear theory based on the local spectrum:

$$B_1 = \frac{\sigma_{1,\text{measured}}}{\sigma_{1,\text{quasi}-\text{determinism}}}, \quad B_2 = \frac{\sigma_{2,\text{measured}}}{\sigma_{2,\text{quasi}-\text{determinism}}}. \tag{14}$$

We then establish B_{mean} and ΔB as parameters describing changes in the group width and the group asymmetry when compared to the linear theory:

$$B_{\text{mean}} = \frac{B_1 + B_2}{2}, \quad \Delta B = B_2 - B_1, \tag{15}$$

A positive value of $1 - B_{\text{mean}}$ suggests the group tends to contract relative to

the shape expected under linear evolution. A positive value of ΔB implies the largest wave tends to move to the front of the group.

Figure 6 shows the evolution of envelope asymmetry for the top 20 largest events in 32 min simulations (approximately 1280 waves) of case 2 in different water depths. Among all of the water depths, we observe a positive value of ΔB, which suggests the largest wave moves to the front of the wave group. Despite the waves propagating in different water depths, the general trends of the evolution of horizontal asymmetry of largest events are similar. ΔB starts at zero as the generated waves are linear random waves. Soon after the wave departs from the relaxation zone, strong wave asymmetry is observed for all cases. This is where the sea-state is furthest from its equilibrium state. The horizontal asymmetry then peaks at slightly different positions for different water depths and settles down to a smaller near-zero steady state value. Waves propagating in shallower water depths seem to have slightly higher asymmetry value at both the peak and the steady state, especially for the shallowest water case ($k_0 d = 1.33$). The length scales of the initial increase for different cases seems to be similar for all the water depths.

Figure 7 shows the average contraction of the wave group around an extreme event given by $1 - B_{\text{mean}}$. We observe a positive value of $1 - B_{\text{mean}}$ for all the cases, which indicates the wave groups tend to contract compared to the evolution under linear theory. Different from the evolution of horizontal asymmetry, the contraction of the wave group increases initially before flattening off when equilibrium is achieved. The contraction occurs on a slightly different spatial scale compared to the horizontal asymmetry, but the spatial scale of initial contraction increase for all different water depths seem to be similar.

In the recent work of [49], comparison of the horizontal asymmetry is made between the deep water case and the shallow water case (their Figure 14). Their results show that for medium and relatively large waves, cases with shallower water depths show more horizontal asymmetry, which agrees well with our results in Figure 6. They also find that, particularly for deep water wave, there is a greater level of horizontal asymmetry for the extremely large waves. To fur-

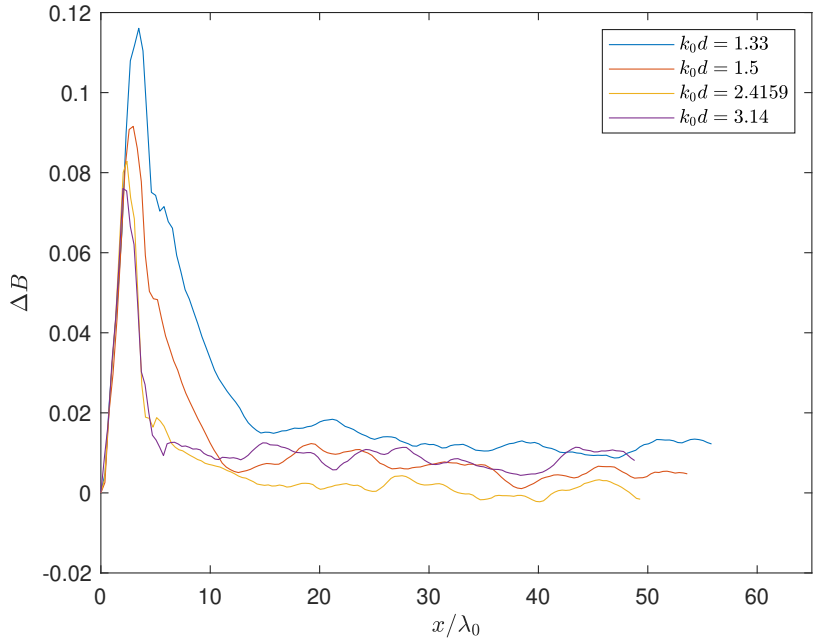

Figure 6: Change in envelope asymmetry (ΔB) for top 20 largest events in each realisation of case 2 with different water depth.

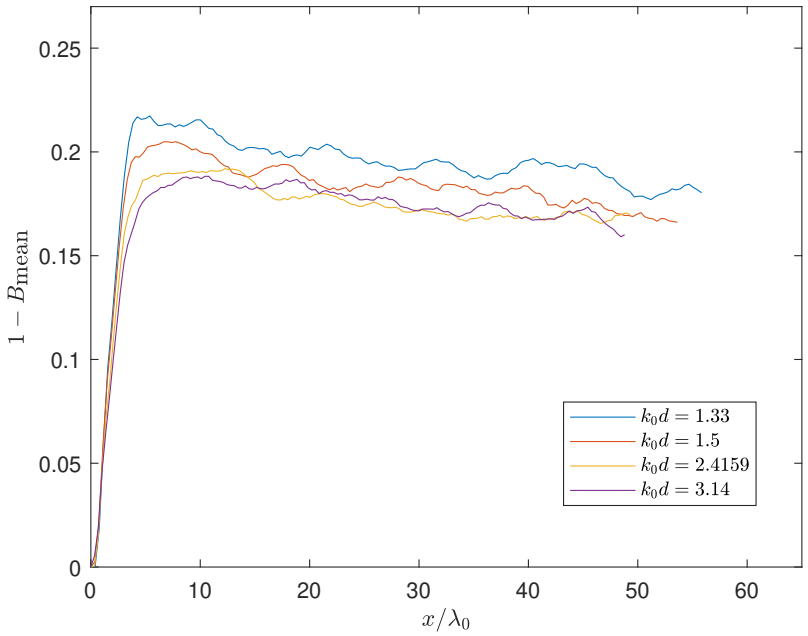

Figure 7: Nonlinear change in the duration when the envelope height of top 20 largest events exceeds 80% of its peak height ($1 - B_{\mathrm{mean}}$) in each realisation of case 2 with different water depth.

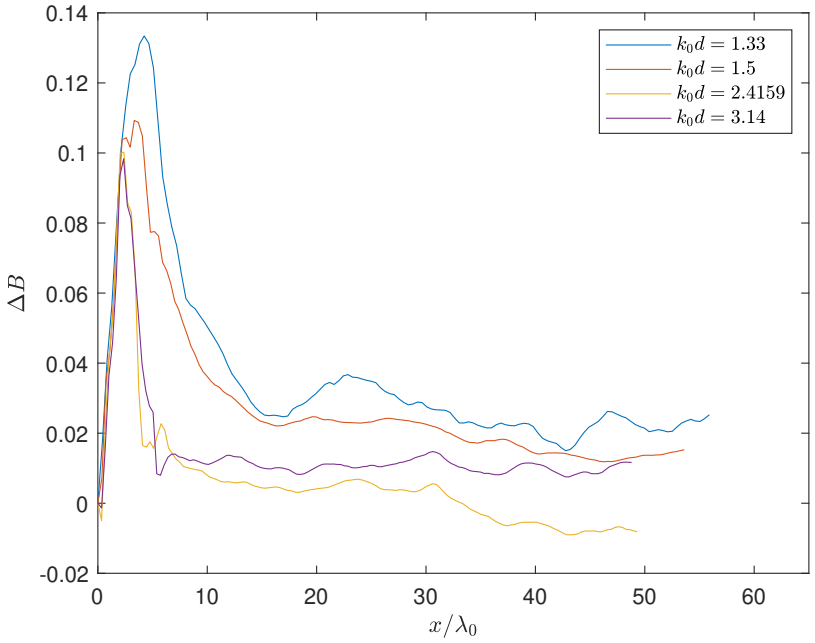

Figure 8: Change in envelope asymmetry (ΔB) for the top 5 largest events in each realisation of case 2 with different water depth.

ther investigate the wave depth effects on extremely large waves, we performed the same data analysis method but only for the top 5 largest waves in a 32 min time series. This will give us the measure of the averaged shape of extreme events with exceedance probability abound 10^-4.

Figure 8 shows the evolution of envelope asymmetry for the top 5 largest events in different water depth. From Figure 8, the overall trends and the spatial scale of the averaged envelope asymmetry of the top 5 largest events are quite similar with that of the top 20 largest events shown in Figure 6. However, the top 5 largest events generally show more significant horizontal asymmetry at the peak and at the steady state. The effect of water depth on the envelope asymmetry is greatly reduced. This observation agrees well with the results in [49].

In addition to the similar horizontal asymmetry results as [49], we further

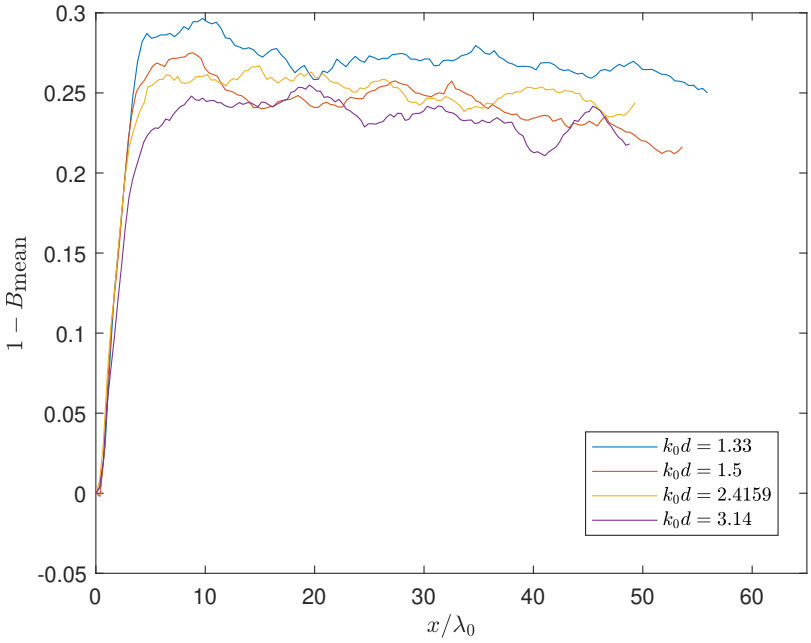

Figure 9: Nonlinear change in the duration when the envelope height of top 5 largest events exceeds 80% of its peak height ($1 - B_{\text{mean}}$) in each realisation of case 2 with different water depth.

investigate the contraction of the envelope for top 5 largest events at different water depth in Figure 9. The general trends are similar to the top 20 largest events shown in Figure 7, except the top 5 largest events have a greater contraction when compared to the top 20 largest events. As such, our results are consistent with the study of [49]

4. Discussion and conclusions

This paper studies how the properties of extreme waves evolve in wave-tanks. We examine both the amplitude of the waves but also the changes to the average shape of an extreme wave group. We use fully non-linear numerical simulations to study these across a variety of depths in intermediate and deep water. For all these parameters, the initial state is not in equilibrium and so these go through

a transient period before settling down to an equilibrium state.

We use the kurtosis of the free surface as a proxy for the number of extreme waves. At the paddle the kurtosis of the linearised signal is 3. In all cases we see an increase in kurtosis down the tank although this is significantly supressed by finite depth effects. This suppression of nonlinear wave focussing agrees well with the previous literature [18, 19, 20] and experiments [25]. This may not be desirable for engineers engaged in model testing in unidirectional flumes since this increase in the number of large waves would not be expected in the open ocean. We have adapted an analytical model to account for finite depth which captures the leading order physics. We propose this as a simple model which could be used by engineers to understand whether an undesirably large number of big waves will occur in their experiments. The effects described in this paper are driven by non-linearity and, unsurprisingly, will be more significant in steeper sea-states. For model testing in directional spread flumes, increase in the number of large waves due to oblique perturbations should also be considered (see results in [22, 23, 24, 25]).

The width and duration of a large wavegroup behaves consistently across all depths. There is a monotonic transition from the initial state to the equilibrium state. There appears to be very little variation in this with depth which is interesting suggesting that the cubic term in the NLS may not be driving this. The greatest contraction appears to be for the shallowest case. This result goes somewhat against the results of Adcock & Yan [50] who studied isolated wave groups and found the contraction was inhibited by depth although not by as much as would be expected using predictions from the cubic NLS. However, our results show that the departure from the shape expected in linear theory is transient and average group shape returns to one close to that predicted by linear theory. Thus, if the group shape is critical in a test, it is suggested the structure to be tested is placed after this transient period (roughly 20 wavelengths away from the paddle).

Our results here are intended as a guide to those undertaking experimental work with random waves although we hope to have made a contribution to

understanding the physics of these processes.

Acknowledgement

TAAA acknowledges funding from funded by UK/China ORE funding (EPSRC/NERC grant EP/R007632/1). The authors thank Prof Paul Taylor (UWA) for his suggestions on aspects of this work and Prof Harry Bingham (DTU) for his assistance with the numerical model.

References

[1] J. Orszaghova, P. H. Taylor, A. G. L. Borthwick, A. C. Raby, Importance of second-order wave generation for focused wave group run-up and overtopping, Coast. Eng. 94 (2014) 63–79.

[2] M. Christou, K. Ewans, Field measurements of rogue water waves, J. Phys. Oceanogr. 44 (9) (2014) 2317–2335.

[3] F. Fedele, On the kurtosis of deep-water gravity waves, J. Fluid Mech. 782 (2015) 25–36.

[4] T. Tang, P. S. Tromans, T. A. A. Adcock, Field measurement of nonlinear changes to large gravity wave groups, J. Fluid Mech. 873 (2019) 1158–1178.

[5] I. Karmpadakis, C. Swan, M. Christou, Assessment of wave height distributions using an extensive field database, Coast. Eng. 157 (2020) 103630.

[6] J. Grue, Two phenomena: Honji instability, and ringing of offshore structures, Theor. App. Mech. Lett. 1 (6) (2011) 062001.

[7] J. Zang, P. H. Taylor, G. Morgan, R. Stringer, J. Orszaghova, J. Grice, M. Tello, Steep wave and breaking wave impact on offshore wind turbine foundations–ringing re-visited, 25th Int. Workshop Water Waves and Floating Bodies, Harbin, China (2010) 9–12.

[8] T. B. Benjamin, J. E. Feir, The disintegration of wave trains on deep water Part 1. Theory, J. Fluid Mech. 27 (3) (1967) 417–430.

[9] P. A. E. M. Janssen, Nonlinear four-wave interactions and freak waves, J. Phys. Oceanogr. 33 (4) (2003) 863–884.

[10] N. Mori, P. A. E. M. Janssen, On kurtosis and occurrence probability of freak waves, J. Phys. Oceanogr. 36 (7) (2006) 1471–1483.

[11] F. Fedele, D. Dutykh, Special solutions to a compact equation for deep-water gravity waves, J. Fluid Mech. 712 (2012) 646–660.

[12] F. Fedele, Z. Cherneva, M. A. Tayfun, C. Guedes Soares, Nonlinear Schrödinger invariants and wave statistics, Phys. Fluids 22 (3) (2010) 036601.

[13] P. A. E. M. Janssen, A. J. E. M. Janssen, Asymptotics for the long-time evolution of kurtosis of narrow-band ocean waves, J. Fluid Mech. 859 (2019) 790–818.

[14] W. Xiao, Y. Liu, G. Wu, D. K. P. Yue, Rogue wave occurrence and dynamics by direct simulations of nonlinear wave-field evolution, J. Fluid Mech. 720 (2013) 357–392.

[15] M. Onorato, A. R. Osborne, M. Serio, L. Cavaleri, C. Brandini, C. T. Stansberg, Extreme waves, modulational instability and second order theory: wave flume experiments on irregular waves, Europ. J. Mech.-B/Fluids 25 (5) (2006) 586–601.

[16] M. Onorato, T. Waseda, A. Toffoli, L. Cavaleri, O. Gramstad, P. A. E. M. Janssen, T. Kinoshita, J. Monbaliu, N. Mori, A. R. Osborne, et al., Statistical properties of directional ocean waves: the role of the modulational instability in the formation of extreme events, Phys. Rev. Lett, 102 (11) (2009) 114502.

[17] A. Toffoli, O. Gramstad, K. Trulsen, J. Monbaliu, E. Bitner-Gregersen, M. Onorato, Evolution of weakly nonlinear random directional waves: laboratory experiments and numerical simulations, J. Fluid Mech. 664 (2010) 313–336.

[18] P. A. E. M. Janssen, M. Onorato, The intermediate water depth limit of the Zakharov equation and consequences for wave prediction, J. Phys. Oceanogr. 37 (10) (2007) 2389–2400.

[19] N. Mori, T. Yasuda, Effects of high-order nonlinear interactions on unidirectional wave trains, Ocean Eng. 29 (10) (2002) 1233–1245.

[20] G. Whitham, Linear and nonlinear waves, John Wiley & Sons (1974).

[21] T. Kakutani, K. Michihiro, Marginal state of modulational instability—note on Benjamin-Feir instability, J. Phys. Soc. Japan 52 (12) (1983) 4129–4137.

[22] L. Fernandez, M. Onorato, J. Monbaliu, A. Toffoli, Modulational instability and wave amplification in finite water depth, Nat. Hazards Earth Syst. Sci. 14 (3) (2014) 705–711.

[23] A. Slunyaev, C. Kharif, E. Pelinovsky, T. Talipova, Nonlinear wave focusing on water of finite depth, Physica D 173 (1-2) (2002) 77–96.

[24] A. Toffoli, L. Fernandez, J. Monbaliu, M. Benoit, E. M. Gagnaire-Renou, J. M. Lefevre, L. Cavaleri, D. Proment, C. Pakozdi, C. T. Stansberg, T. Waseda, M. Onorato, Experimental evidence of the modulation of a plane wave to oblique perturbations and generation of rogue waves in finite water depth, Phys. Fluids 25 (9) (2013) 091701.

[25] A. Toffoli, M. Benoit, M. Onorato, E. M. Bitner-Gregersen, The effect of third-order nonlinearity on statistical properties of random directional waves in finite depth, Nonlinear Process Geophys. 16 (1) (2009) 131–139.

[26] L. Fernandez, M. Onorato, J. Monbaliu, A. Toffoli, Occurrence of extreme waves in finite water depth, in: Extreme ocean waves, Springer, 2016, pp. 45–62.

[27] I. Karmpadakis, C. Swan, M. Christou, Laboratory investigation of crest height statistics in intermediate water depths, Proc. R. Soc. A Math. Phys. Eng. Sci. 475 (2229) (2019) 20190183.

[28] A. P. Engsig-Karup, H. B. Bingham, O. Lindberg, An efficient flexible-order model for 3D nonlinear water waves, J. Comp. Phys. 228 (6) (2009) 2100–2118.

[29] D. Barratt, H. B. Bingham, T. A. A. Adcock, Nonlinear evolution of a steep, focusing wave group in deep water simulated with OceanWave3D, J. Offshore Mech. Arct. Eng. 142 (2) (2020).

[30] T. Tang, W. Xu, D. Barratt, H. B. Bingham, Y. Li, P. H. Taylor, T. S. van den Bremer, T. A. A. Adcock, Spatial evolution of the kurtosis of steep unidirectional random waves, J. Fluid Mech. 908 (2021).

[31] S. A. Hughes, The TMA shallow-water spectrum description and applications, Tech. rep., Coastal Engineering Research Center (US) (1984).

[32] C. N. Whittaker, A. C. Raby, C. J. Fitzgerald, P. H. Taylor, The average shape of large waves in the coastal zone, Coast. Eng. 114 (2016) 253 – 264.

[33] D. Barratt, H. B. Bingham, T. S. van den Bremer, T. A. A. Adcock, Linearization of the wave spectrum: A comparison of methods, 39th Int. Ocean Offshore Arct. Eng. Conf., Florida, USA (2020).

[34] M. Serio, M. Onorato, A. R. Osborne, P. A. E. M. Janssen, On the computation of the Benjamin-Feir Index, Nuovo Cim. della Soc. Ital. di Fis. C 28 (6) (2005) 893–903.

[35] C. C. Mei, The Applied Dynamics of Ocean Surface Waves, volume: 1 Edition, World Scientific Publishing Co. Pte. Ltd, New York, 1989.

[36] Y. Goda, Random seas and design of maritime structures, World scientific, 2000.

[37] C. X. K. Prasada Rao, Spectral width parameter for wind-generated ocean waves, Proc. Indian Acad. Sci. - Earth Planet. Sci. 97 (2) (1988) 173.

[38] M. Onorato, A. R. Osborne, M. Serio, L. Cavaleri, C. Brandini, C. T. Stansberg, Observation of strongly non-Gaussian statistics for random sea surface gravity waves in wave flume experiments, Phys. Rev. E 70 (6) (2004) 067302.

[39] A. Toffoli, J. Monbaliu, M. Onorato, A. R. Osborne, A. V. Babanin, E. Bitner-Gregersen, Second-order theory and setup in surface gravity waves: a comparison with experimental data, J. Phys. Oceanogr. 37 (11) (2007) 2726–2739.

[40] A. Toffoli, M. Onorato, E. Bitner-Gregersen, A. R. Osborne, A. Babanin, Surface gravity waves from direct numerical simulations of the euler equations: a comparison with second-order theory, Ocean Eng. 35 (3-4) (2008) 367–379.

[41] P. A. E. M. Janssen, J. R. Bidlot, On the extension of the freak wave warning system and its verification, ECMWF Tech. Mem. 588 (2009).

[42] G. Lindgren, Some properties of a normal process near a local maximum, Ann. Math. Statist 41 (6) (1970) 1870–1883.

[43] P. Boccotti, Some new results on statistical properties of wind waves, Appl. Ocean Res. 5 (3) (1983) 134–140.

[44] P. S. Tromans, A. R. Anaturk, P. Hagemeijer, A new model for the kinematics of large ocean waves-application as a design wave, 1st Int. Offshore and Polar Eng. Conf., Edinburgh, UK (1991).

[45] T. E. Baldock, C. Swan, P. H. Taylor, A laboratory study of nonlinear surface waves on water, Philos. Trans. R. Soc. A 354 (1707) (1996) 649–676.

[46] T. A. A. Adcock, P. H. Taylor, Focusing of unidirectional wave groups on deep water: an approximate nonlinear Schrödinger equation-based model, Proc. R. Soc. A Math. Phys. Eng. Sci. 465 (2110) (2009) 3083–3102.

[47] E. Lo, C. C. Mei, A numerical study of water-wave modulation based on a higher-order nonlinear Schrödinger equation, J. Fluid Mech. 150 (1985) 395–416.

[48] G. Dematteis, T. Grafke, M. Onorato, E. Vanden-Eijnden, Experimental evidence of hydrodynamic instantons: the universal route to rogue waves, Phys. Rev. X 9 (4) (2019) 041057.

[49] I. Karmpadakis, C. Swan, On the average shape of the largest waves in finite water depths, J. Phys. Oceanogr. 50 (4) (2020) 1023–1043.

[50] T. A. A. Adcock, S. Yan, The focusing of uni-directional Gaussian wave-groups in finite depth: an approximate NLSE based approach, in: 29th Int. Ocean Offshore Arct. Eng. Conf., Shanghai, China, Vol. 49125, 2010, pp. 569–576.